Effect of wavelength and defect density on the efficiency of InGaN based light emitting diodes

Markus Pristovsek,* An Bao, and Rachel A. Oliver
Department of Materials Science and Metallurgy, University of Cambridge, 27 Charles Babbage Road, Cambridge, CB3 0FS, UK

Tom Badcock,† Muhammad Ali,‡ and Andrew Shields
Toshiba Research Europe Ltd., Cambridge Research Laboratory, 208 Science Park, Milton Road, Cambridge, CB4 0GZ, UK

We measured the electro-luminescence of light emitting diodes (LEDs) on substrates with low dislocation densities (LDD) at $10^6\,\mathrm{cm}^{-2}$ and low $10^8\,\mathrm{cm}^{-2}$, and compared them to LEDs on substrates with high dislocation densities (HDD) closer to $10^{10}\,\mathrm{cm}^{-2}$. The external quantum efficiencies (EQEs) were fitted using the ABC-model with and without localisation. The non-radiative recombination (NR) coefficient A was constant for HDD LEDs, indicating that the NR was dominated by dislocations at all wavelengths. However, A strongly increased for LDD LEDs by a factor of twenty when increasing the emission wavelength from 440 nm to 540 nm. We attribute this to an increased density of point defects due to the lower growth temperatures used for longer wavelengths. The radiative recombination coefficient B followed the squared wave function overlap for all samples. Using the observed coefficients, we calculated the peak efficiency as a function of the wavelength. For HDD LEDs the change of wave function overlap (i.e. B) is sufficient to reduce the EQE as observed, while for LDD LEDs also the NR coefficient A must increase to explain the observed EQEs. Thus reducing NR is important to improve the EQEs of green LEDs, but this cannot be achieved solely by reducing the dislocation density: point defects must also be addressed.

I. INTRODUCTION

Many efforts are under way to improve the external quantum efficiency (EQE) of InGaN-based LEDs. Currently such LEDs are usually produced either on (0001) sapphire or (111) silicon substrates by hetero-epitaxy. This typically results in a threading dislocation density (TDD) of low $10^8\,\mathrm{cm}^{-2}$ on sapphire and closer to $10^9\,\mathrm{cm}^{-2}$ on silicon. The variation in TDD has an impact on the EQE, which was shown for LEDs emitting at wavelengths shorter than 460 nm [1–6].

Apart from the TDD, the efficiency of nitride LEDs decreases at wavelengths longer than 480 nm. This is often referred to as the "green gap". One explanation which is often put forward is a slower radiative recombination rate due to a reduced overlap between the electron and hole wave function which is caused by a larger piezoelectric field from a larger strain with higher In content. However, recent reports on LEDs [7], laser diodes [8], and photo-luminescence (PL) of quantum wells (QWs) [9, 10] found that non-radiative recombination also increases at longer wavelengths. A comparison of QWs with the same wavelength and structural parameters but grown at different temperatures showed that the resulting internal quantum efficiency (IQE) strongly depends on growth temperature. This suggests that non-radiative losses are not strain driven [10, 11].

In order to quantify the influence of wave function overlap and TDD on non-radiative recombination and the green gap, we investigated LEDs over a wide wavelength range, using three different basic templates with very different dislocation densities. The obtained coefficients are used to model the EQE of LEDs with different dislocation densities to provide an insight into the origin of the green gap.

II. EXPERIMENTAL

All the LEDs were grown by metal-organic vapour phase epitaxy. The lowest dislocation density was for freestanding GaN substrates, obtained from Kyma technologies. Low dislocation density (LDD) templates were grown on (0001) sapphire with an optimised low temperature nucleation around 530°C, followed by annealing at 1050°C. Growth was initiated by conditions which encouraged the formation of three-dimensional islands, followed by island coalescence as described in ref. [12]. For high dislocation density samples (HDD) the nucleation and annealing times were shortened, and conditions used which promoted two-dimensional growth after the annealing step [12]. TDDs were obtained from the density of dark spots in scanning electron microscope cathodoluminescence (SEM-CL) for freestanding GaN and LDD, while for the HDD growth the TDD related surface pits were counted in atomic force microscopy [13]. Typical TDDs were below $10^7\,\mathrm{cm}^{-2}$ for freestanding GaN,

* pristovsek@nagoya-u.ac.jp; Current address: Center for Integrated Research of Future Electronics, Institute for Materials and Systems for Sustainability, Nagoya University, 1 Furo-cho, Chikusa-Ku, Nagoya, 464-8603, Japan
† Current address: Oclaro Technology Ltd., Caswell, Towcester, NN12 8EQ, UK
‡ Current address: Osram Opto Semiconductors GmbH, Leibnizstr. 4, 93055 Regensburg, Germany

$2-4\times10^8\,\mathrm{cm}^{-2}$ for LDD, and close to $10^{10}\,\mathrm{cm}^{-2}$ for HDD.

For the HDD LEDs the thickness of the n-doped side was limited to $1\,\mu$m, because thicker layers cracked due to high (10^{-3}) in-plane tensile strain, as determined by X-ray diffraction (XRD). Hence, to maintain a comparable LED structure, the thickness of the n-doped side was limited to $1.5\,\mu$m for the LEDs on freestanding GaN and LDD. In order to span a wavelength range from blue to green without changing the nominal structure, only three quantum wells (QWs) were used. QW growth was carried out entirely with nitrogen carrier gas and trimethylindium and tri-ethylgallium precursors. The GaN barriers were grown under a 99:1 nitrogen:hydrogen mixture about 80°C higher than the QWs, and the temperature was increased immediately after the end of the QW. This so-called two temperature (2T) strategy [14] minimizes the formation of trench defects at longer emission wavelengths which may otherwise control the EQE [15]. Indeed, we observed less than $10^7\,\mathrm{cm}^{-2}$ trench defects and no change in TDD for multiple QWs (MQWs) without a p-GaN cap emitting at 545 nm by SEM-CL. XRD showed fully strained layers in reciprocal space maps. TEM showed QWs with few thickness fluctuations and nice interfaces. No dislocations were generated in the MQWs even in the LED at 532 nm on the freestanding GaN template.

No electron blocking layer was used; the last barrier was covered with 140 nm of p-GaN and 20 nm of p++ GaN, grown at the relatively low susceptor surface temperature of 900°C. The LEDs were processed into devices with five different p-contact geometries in different sizes, using Ni/Au transparent contact (4.5/4.5 nm annealed at 450°C in O_2+N_2 for 5 min) with Ti/Au pads (20/80 nm) as p-contacts and Ti/Al/Ti/Au (15/50/30/80 nm annealed at 700°C in N_2 for 60 s) as n-contacts. The electroluminescence (EL) was measured on-chip by backside collection using an integrating sphere with two different detectors, or from the front using an optical fibre. For each wavelength and template at least four different devices were measured and analysed.

The wave function overlap integral was calculated as described in ref. [16], assuming a bowing parameter of 1.7 and a QW thickness of 3.0 nm.

III. RESULTS AND DISCUSSION

A. Theory

The emission of LEDs is commonly described by the ABC-model [7, 17–19]. The current I is connected to the carrier density n by

$$N(n) := I(n)\frac{\eta_{inj}}{e_0 V} = (An + Bn^2 + Cn^3) \qquad (1)$$

where N is the total recombination rate, the coefficient A is attributed to the Shockley—Read-–Hall (SRH) non-radiative recombination, B gives the radiative free carrier (electron+hole) recombination, and C is the carrier activated loss (often assumed to be Auger related). V, the volume of the active region, is given by $V = dS$, where d the thickness of the QW, S the area of the device, e_0 the elementary charge, and η_{inj} the injection efficiency.

For the analysis, we assume that the light output is only given by the radiative recombination. Optical losses between the QW and the detector are accounted for by the extraction efficiency $\eta_e \leq 1$. Then the light output L (the number of emitted photons per time) is given by the radiative recombination rate in the active volume

$$L(n) = \eta_e V B n^2. \qquad (2)$$

The EQE is defined as the number of photons detected divided by the number of injected carriers

$$EQE(n) = L(n)\frac{e_0}{I(n)} = \eta_e\eta_{inj}\frac{Bn^2}{An + Bn^2 + Cn^3}. \qquad (3)$$

For $\eta_e = \eta_{inj} = 1$ the EQE is identical to the internal quantum efficiency (IQE). In eq. (3) any increase of the coefficients A or C would reduce the peak (maximum) EQE. From theory, a higher TDD should increase A, because the SRH recombination only depends on the density of non-radiative centres and the carrier density. The other loss C is a three carrier process ($\propto n^3$). As such it is only relevant when there is a high local carrier density, at which point the SRH recombination centres will be mostly saturated. Therefore, C is expected to be largely independent of the TDD. Indeed, experimentally C was nearly constant over a large wavelength range [7] or various In contents and QW thicknesses [20].

The most important process is the radiative emission. Its coefficient B is related to the square of the wave function overlap [7], which is determined by the In content in the QW and the barrier, the QW thickness, and the substrate orientation. If free carriers recombine when they randomly meet, the radiative recombination is proportional to the product of electron and hole densities n^2. However, electrons can be localised at QW thickness fluctuations or holes at random alloy fluctuations [21]. Then the electron and hole are captured subsequently and the radiative recombination becomes proportional to the carrier density n, i.e. the chance of a carrier meeting a localisation site. In the localised case, the number of generated photons is $\eta_e V B_l n$(where B_l is the localised recombination rate), and the EQE becomes

$$EQE = \eta_e\eta_{inj}\frac{B_l n}{An + B_l n + Cn^3}, \qquad (4)$$

assuming the carrier activated loss still scales like n^3.

Fig. 1 shows the obtained EQE curves. With localisation the EQE has its maximum at zero carrier density with $EQE(0) = \eta_e\eta_{inj}\frac{B_l}{A+B_l}$ (since non-radiative as well as radiative recombination are both linear in n). At higher carrier densities the additional Auger losses start

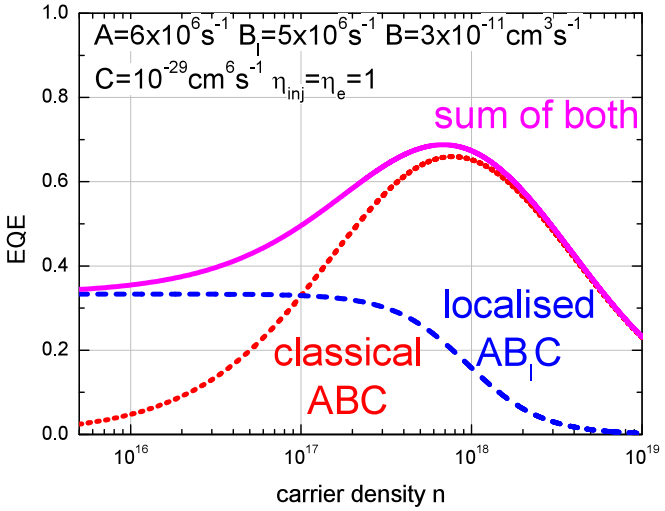

FIG. 1. Shape of EQE curves for the classical case with $L \propto n^2$ (eq. 3, dotted) and the localised case with $L \propto n$ (eq. 4, dashed) and a sum of both for typical coefficients.

to reduce the localised EQE. On the other hand, without localisation the EQE goes to zero for small carrier densities. If both recombination processes occur simultaneously, then localisation will dominate at low carrier densities.

An earlier time dependent PL study found that localisation could be only modelled reasonably well if either an excess of holes or electrons are localised [22]. Thus, it is no surprise that the shape of the EQE for the sum of both recombination processes in fig. 1 (solid) is very similar to the EQE obtained by background doping [19, 23], i.e. when one carrier type is in abundance. For background doping the radiative recombination becomes $\propto n$ at low carrier densities. For typical ABC coefficients Karpov et al. estimated that an excess (i.e. localisation site density) of $5 \times 10^{18}\,\mathrm{cm}^{-3}$ is needed to dominate recombination up to the maximum EQE (fig. 3 in ref. [23]). This rather high number of localisation sites explains why typical EQE curves are closer to the classical EQE shape.

Mathematically, fitting an experimental EQE with a sum of eq. (3) and (4) is difficult, since A and B_l are strongly interdependent. But fig. 1 also shows that even for a large B_l the sum can still be approximated by the non-localised classical eq. (3) for carrier densities starting shortly before the maximum EQE, although this slightly overestimates A. Thus, if there is still a clear maximum, then the EQE curve can be described with a small error by eq. (3) around the maximum.

A fundamental assumption of the ABC model is, that the three coefficients A, B, and C are constant. However, there are recent indications that this is not necessarily the case, for instance the non-radiative lifetime (inverse of A) increases with increasing carrier density [24–26]. Also the radiative recombination is expected to increase at high current densities, when screening of the internal fields in the QW increases the wave function overlap (and thus B). Other effects compete with this, namely carrier activated defect recombination [27] or hole degeneration in QWs [23]. (The latter reduces B by hole degeneration $\propto \frac{1-\exp(-\frac{n}{D})}{n\tau_r}$, with D the density of states in the QW, and τ_r the radiative lifetime [23].) Furthermore, even the injection efficiency η_{inj} decreases at high carrier densities [28, 29]. Since all these effects compete, the classical ABC-model (assuming constant coefficients) reaches its limits at high carrier densities. Still, the ABC-model fits experimental EQE curves of many LEDs very well around the EQE maximum. Within the limitations of the model, analysis of the systematic variation of the A, B, and C coefficients should facilitate further understanding of the green gap.

A direct fitting of the EQE with eq. (3) is not possible, since the carrier density is given by $\sqrt{L} = \sqrt{\eta_e B} n$, but neither B nor η_e are known. Since the light output is proportional to the carrier density squared, one defines the new independent variable $x = \sqrt{L/L_{peak}}$ with L_{peak} the light output at maximum EQE. By also defining $P = \frac{B}{\sqrt{AC}}$ and rearranging eq. (3) [18] one finally obtains

$$\frac{EQE(x)}{EQE_p} = \frac{P+2}{P+\frac{1}{x}+x}. \tag{5}$$

The three fitting parameter are very independent, the shape is entirely given by P, the amplitude is EQE_p and the maximum position is L_{peak}, and there is very little cross coupling between these.

From P the maximum IQE_{peak} can be calculated

$$IQE_{peak} = \frac{P}{P+2} = \frac{B}{B+\sqrt{AC}} \tag{6}$$

and from that follows the extraction and injection efficiencies

$$\eta_e \eta_{inj} = \frac{1}{IQE_{peak} EQE_p} = \frac{P+2}{P\,EQE_p}. \tag{7}$$

At IQE_{peak}, the first derivate of eq. (3) is zero i.e. $\frac{d}{dn} EQE = 0$. The only meaningful solution is

$$n_{peak} = \sqrt{\frac{A}{C}}, \tag{8}$$

which can be put into eq. (1) and (3) to obtain values for the coefficient A, B, or C when fixing one of them. Using $N_{peak} = N(n_{peak}) = I_{peak} \frac{\eta_{inj}}{e_c V}$ one obtains finally

$$\begin{aligned} N_{peak}(1 - IQE_{peak}) &= 2\frac{N_{peak}}{P+2} = 2\sqrt{\frac{A^3}{C}} \\ \frac{N_{peak}}{4}\frac{(1-IQE_{peak})^2}{IQE_{peak}} &= \frac{N_{peak}}{P(P+2)} = \frac{A^2}{B} \end{aligned} \tag{9}$$

or as dependence from C

$$\frac{4N_{peak}(IQE_{peak})^3}{(1-IQE_{peak})^2} = \frac{N_{peak}P^3}{P+2} = \frac{B^3}{C^2}. \tag{10}$$

For very low excitation one can neglect the C term in eq. (1) completely: $I \approx \frac{e_0 V}{\eta_{inj}}(An + Bn^2)$. From eq. (2) one can express the carrier density by the light output $n = \sqrt{\frac{L}{\eta_e B V}}$ and replace I by $\frac{L e_0}{EQE}$ (eq. 3). With this one obtains:

$$\frac{1}{EQE} \approx \frac{1}{\eta_{inj}\eta_e} + \frac{A}{\eta_{inj}}\sqrt{\frac{V}{\eta_e B L}}. \tag{11}$$

This was first derived by Opdorf and 't Hooft [30]. Fitting a line to the low current data of EQE^{-1} over $L^{-\frac{1}{2}}$ gives the slope and the intercept. The latter is the reciprocal of $\eta_e\eta_{inj}$, although the η_e is about a factor of two smaller compared to eq. (7), since it is obtained by extrapolating to large currents, where non-linear C losses cannot be neglected. This method works best for $L \ll L_{peak}$, more than a factor of 100 away from the peak EQE, and one has to be careful that the device does not show localisation.

The slope Sl in eq. (11) is given by $\frac{A}{\eta_{inj}}\sqrt{\frac{V}{\eta_e B}}$. Rearranging this we get

$$\frac{\eta_{inj}^2\eta_e}{V} Sl^2 = \frac{A^2}{B} \tag{12}$$

which can be directly compared with eq. (9). Indeed, the eq. (12) and (9) agree when using the same η_e and η_{inj}. The method does not rely on the C coefficient, which is important since there is some disagreement about the value of C in literature (as discussed in the next section).

Eq. (9), (10), or (12) require prior knowledge of B to calculate the other coefficients A and C. An independent way to obtain B was first described by Eliseev et al. [31]. It uses frequency dependent small signal modulated EL to obtain the differential carrier lifetime τ: The derivative of eq. (1) to n is $\frac{1}{\tau} = \frac{\partial N}{\partial n} = A + 2Bn + 3Cn^2$. For small carrier densities ($I \ll I_{peak}$) one can ignore the Cn^2 term, and after squaring one obtains $\tau^{-2} = A^2 + 4B(An + Bn^2)$. Since $(An + Bn^2)$ is proportional to the injected current in this regime, then τ is given by $\tau^{-2} = A^2 + \frac{4B\eta_{inj} I}{e_0 V}$. Thus from measurements at different currents, one can get B from the first derivative to the current I

$$B = \frac{e_0 V}{4\eta_{inj}} \frac{\partial}{\partial I} \tau^{-2} \tag{13}$$

using the same volume V and injection efficiency η_{inj} as before.

This leaves us with the last unknown, the injection efficiency η_{inj}. Calculations have shown that $\eta_{inj} > 90\,\%$ is realistic for 480 nm MQWs at low excitation close to IQE_{peak} but decreases at higher currents [28, 29] and also decreases at higher temperatures or with single QWs [32]. Thus a constant η_{inj} is a reasonable assumption at the small current densities for MQWs as in our study. So we quantify η_{inj} by assuming an ideal injection for the sample with the largest $\eta_e\eta_{inj}$ in our wavelength series. Any reduction in $\eta_e\eta_{inj}$ is then solely assigned to a decrease of η_{inj}. Thus, when comparing to other experimetnal results, one should allow for a scaling of

$$A' = \sqrt{k}A, \quad B' = kB, \quad C' = k^{3/2}C \tag{14}$$

with a scaling constant k due to uncertainties in active volume and peak injection efficiency of the reference sample.

B. Results

The first parameter to determine is the volume of the active region. Since the extracted mean QW thicknesses from TEM agreed well with the values from XRD, we will use a width of 3 nm per QW for all samples. Since there are three QWs in the LEDs the total thickness is 9 nm. While most publications use the same approach, some assume a smaller active region due to the smaller region with a high wave function overlap (e.g. ref. [33]). Furthermore, the carrier density in all QW may be not equal and thus also altering the effective thickness used for calculating the carrier densities. Hence, there is already a systematic deviation of the absolute values of the ABC coefficients in literature from the different definitions of the active region.

Fig. 2 shows typical measured EQE curves at different wavelengths and their fits using eq. (5). Most deviations between measurements and fits were found at low currents, e.g. in fig. 2 for the freestanding and LDD at 470 nm. These EQEs could be simulated by assuming localisation (eq. (4), see fig. 1), although then A and B_l become interdependent and a unique combination of coefficients can not be obtained. If one instead starts the fitting at slightly higher currents closer to the EQE maximum, then these EQEs can be still fitted with eq. (5).

At the longest wavelength, above 540 nm, the EQE curves were very broad, with an asymmetric maximum, and sometimes even a second shoulder at lower currents, as well as strong localisation-like shape. While a broad maximum would correspond to a high IQE, the detected absolute light output was rather low. Moreover, the entire shape of the curve was not fitted well. Therefore, we may have reached the usable limits of the ABC-model at 540 nm, as discussed before.

Despite the deviations, the fitting was successful for most of the LEDs at shorter wavelengths: There were only two device series, where the peak IQE strongly deviated from the trend (in fig. 3 on freestanding GaN at 472 nm and one contact geometry at 508 nm). In these both cases the fit at low and at high currents deviated and thus affected the fitted IQE. Otherwise the peak IQE in fig. 3 from the fitting shows the same wavelength dependent trends as seen in the EQE curves in fig. 2, i.e. the peak IQE/EQE is decreasing towards green, and the current density at maximum EQE was shifted to higher currents for lower EQEs.

Fig. 4 (a) shows the combined efficiency $\eta_e\eta_{inj}$ from the fitting. Since the structures of all LEDs were similar,

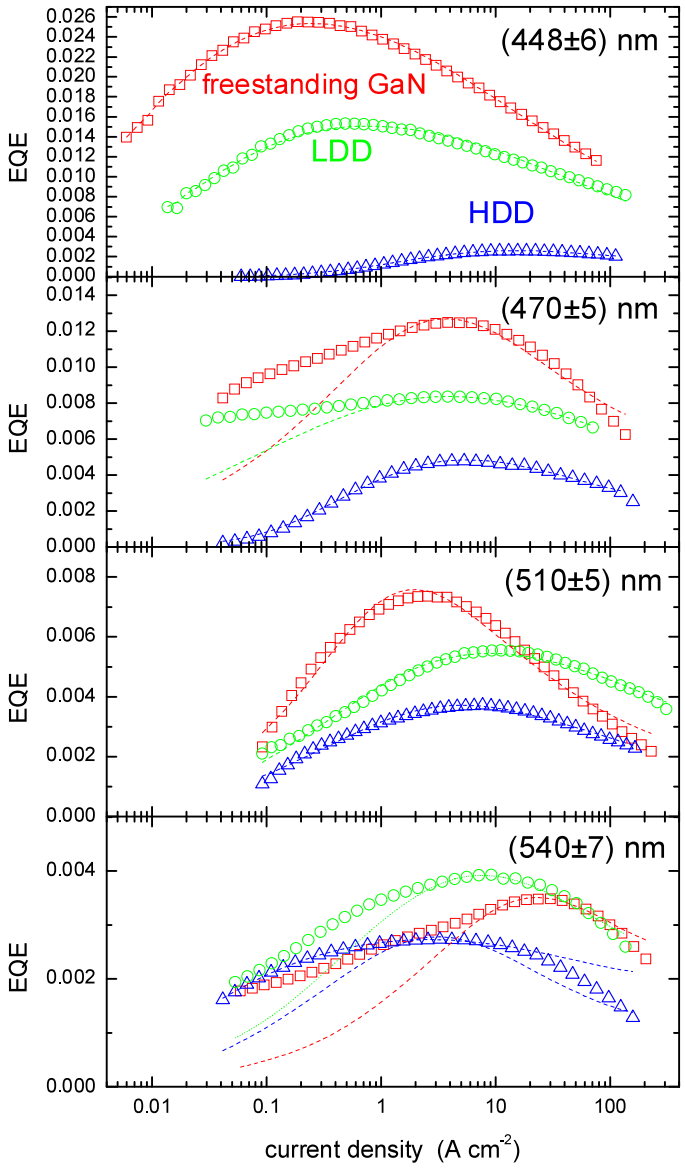

FIG. 2. EQE curves as a function of current density, measured on chip at four different wavelengths on freestanding GaN (□), LDD (○), and HDD (△). Dotted lines are the fits using eq. (5) and converted back to J. The divisions of the y-axis are always 0.002 arbitrary units. For the longest wavelength LEDs (bottom) the shapes strongly deviate from the ideal ABC curve as both fits of emphasizing the low current end (dashed) or of the high current end (dotted) were not good.

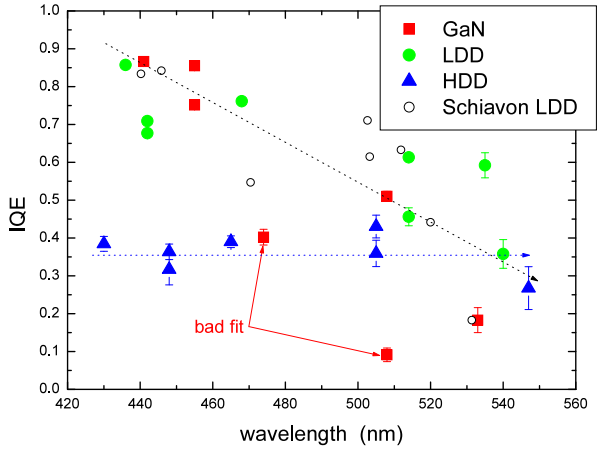

FIG. 3. Mean peak IQE from fitting and eq. (6). The bars are the statistical errors from measuring all devices at that wavelength. The ○ are LDD LEDs on sapphire by Schiavon et al. [7] and calculated from the A, B, and C coefficients using eq. (6).

the extraction efficiency η_e is expected to be almost constant. Only self-adsorption in the p-GaN may somewhat reduce η_e towards longer wavelengths. However, most other losses like carrier bypassing the QW at V-defects and other QW defects, non-uniform injection, or carrier overflow will reduce the injection efficiency η_{inj}. Since the latter is needed for further analysis, we conservatively assumed a wavelength independent extraction efficiency η_e given by the maximum of $\eta_e\eta_{inj}$ for each template type. Then any reduction of $\eta_e\eta_{inj}$ is due to injection losses. The so obtained injection efficiencies η_{inj} have their peak value in fig. 4 (b) around 450 nm. Since our LEDs neither had an electron blocking layer nor an InGaN underlayer below the QWs, the reduction of η_{inj} at shorter wavelengths is probably caused by QWs which become too shallow for efficient injection and carriers start to overflow. A similar reduction of η_{inj} has been reported when the internal fields are reduced in semi-polar QWs [34]. As mentioned before, the reduction of η_{inj} towards longer wavelengths is likely caused by η_e due to self-adsorption in the p-GaN, i.e. to a reduced extraction efficiency η_e. However, its variation is small compared to the one of the A or B coefficients.

Now, we can finally derive values for A, B, and C. First we calculate B using eq. (13) from the modulated EL measurements at low current densities [crossed symbols in fig. 5 (b)]. Because localisation has the strongest impact at low carrier densities (as discussed), this technique worked only for few devices and contact geometries. The resulting B coefficients are mostly in the range of $1-4\times10^{11}\,\mathrm{cm^3s^{-1}}$ which is a commonly reported range [4, 20, 33]. $B = 6\times10^{11}\,\mathrm{cm^3s^{-1}}$ was reported for a green LED using the same technique [31].

Putting the obtained B into eq. (10) yields the C coefficients in fig. 5 (c), which scatter around $10^{-29}\,\mathrm{cm^6s^{-1}}$ with no clear wavelength dependence. A nearly wavelength independent C was observed in literature using direct fitting [20], or the high current differential carrier lifetimes [7, 36, 37]. In literature the C coefficient is often reported around $10^{-29}\,\mathrm{cm^6s^{-1}}$ for measurements on MQWs structures [31, 36, 37] and $< 10^{-31}\,\mathrm{cm^6s^{-1}}$ for single QWs [7, 29]. Since all these values are obtained from modulation measurement, the most likely explanation is a non-uniform carrier distribution among the MQWs especially at low currents, which results in a larger apparent C coefficient for MQWs. Since we mea-

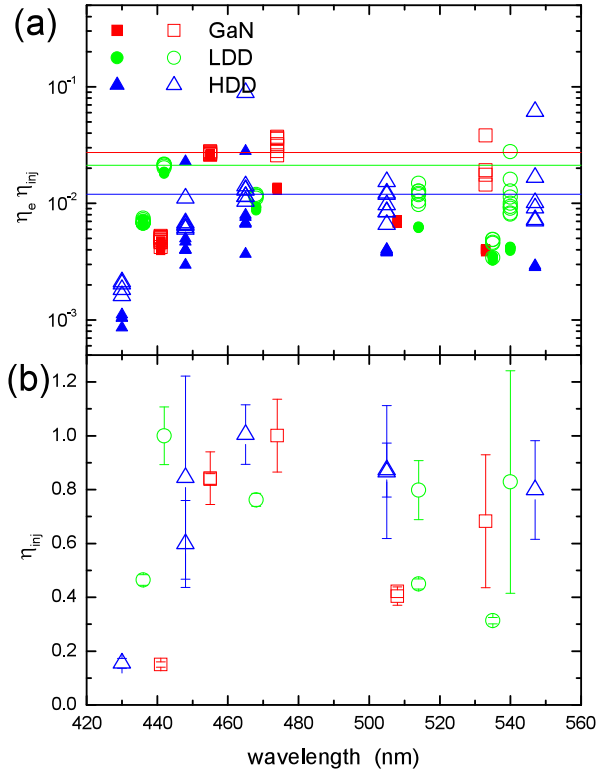

FIG. 4. (a) Efficiencies $\eta_e\eta_{inj}$ from eq. (7) with their mean peak value indicated as lines. (b) Injection efficiencies η_{inj} assuming that the reduction to the peak value is only caused by a reduced injection efficiency.

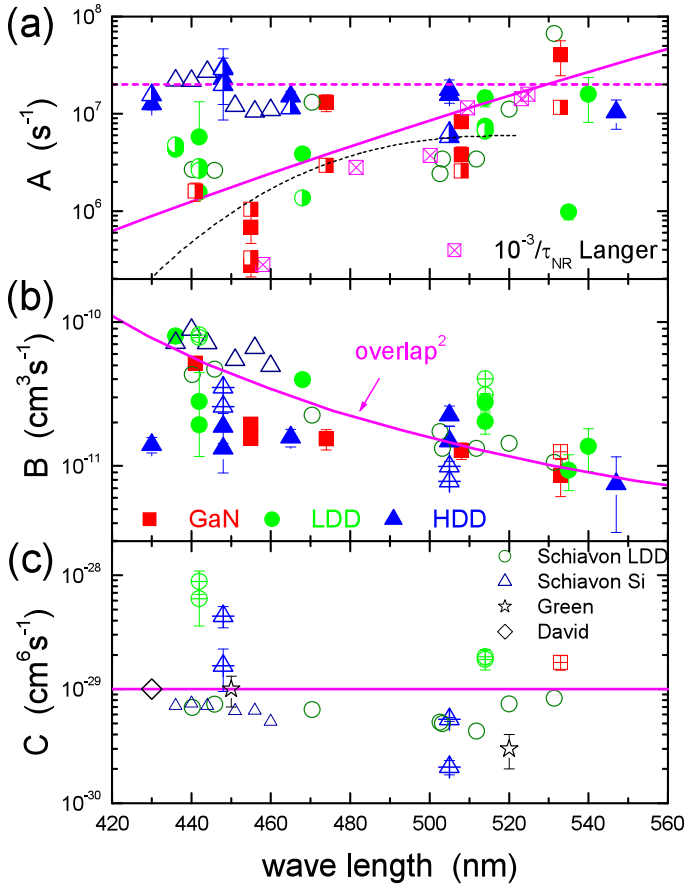

FIG. 5. ABC coefficients points assuming $C = 10^{-29}\,\mathrm{cm^6s^{-1}}$ on freestanding GaN (■), LDD (●), and HDD (▲) or open symbols for coefficients for LDD on sapphire (□) and HDD-like on Si (△) from Schiavon et al. [7], both shifted by $k = 16$ as in eq. (14). The thick solid/dotted lines mark the ideal dependence of A, B, and C which is used to model HDD/LDD LED IQEs. (a) Extracted coefficient A from eq. (9). The freestanding GaN/LDD A increase similar to the reverse non-radiative lifetimes (⊠) of 5× QWs from Langer et al. [9], and also follow the calculated A coefficients for non-radiative recombination at gallium vacancy-oxygen complexes (black dashed line from Alkauskas et al. [35]). The half-filled symbols are calculated using eq. (12). (b) Extracted coefficients B from eq. (10) or directly from differential carrier lifetimes (⊞ ⊕ ⧋) using eq. (13). The line is the squared overlap between electron and hole wave functions for 3.0 nm QWs normalised to $1.5 \times 10^{-11}\,\mathrm{cm^3s^{-1}}$ at 500 nm. (c) Extracted C coefficient from differential carrier lifetimes and eq. (10), the ⋆ are from [36], and ⋄ from [37].

sured MQWs and furthermore focussed on the A and B coefficients, the absolute value of C is not critical: It just scales A and B according to eq. (14) but gives the same EQE. Therefore, we choose $C = 10^{-29}\,\mathrm{cm^6s^{-1}}$ to calculate A and B from eq. (9). Since we use a different C value, in the following the single QW results of Schiavon et al. were scaled by $k = 16$ using eq. (14). Again, the scaling has no impact for the analysis in this paper on the contribution of A and B to the green gap. Furthermore, eq. (12) allows to determine A only from B, and those values were consistent with the A calculated from eq. (9).

The obtained A coefficients in fig. 5 (a) are almost constant for high defects densities (HDD) at a level slightly above $10^7\,\mathrm{s^{-1}}$. They are also close to the values for the GaN on Si LEDs [△ in fig. 5 (a)], which had about six times higher dislocation densities than the LDD ones [7]. For the LDD LEDs either on freestanding GaN or LDD on sapphire, the A coefficients steeply increase from below $10^6\mathrm{s^{-1}}$ at 440 nm to $2 \times 10^7\mathrm{s^{-1}}$ at 530 nm. Again, a similar trend is visible in the LDD data from Schiavon et al. [7] [○ in fig. 5 (a)].

For blue emission, a strong increase of A with increasing defect density was reported previously [4, 20]. However, most striking is that the difference in A of more than a factor of ten between LDD and HDD vanishes towards longer wavelengths. Instead A increases on LDD LEDs by a factor of ten from blue to green while A remain almost constant for HDD LEDs. Thus on HDD LEDs, the non-radiative recombination A is likely limited by the dislocation density, which is wavelength independent and A is insensitive to other non-radiative recombination centres with lower density.

The increase of A for LDD LEDs would indicate that there are indeed other non-radiative recombination cen-

tres whose density increases towards the green. Indeed, Langer et al. directly observed a shortening of the non-radiative lifetime towards green [9] (⊠ in fig. 5). The increase was even stronger than for our data, which may be related to thinner QWs in their experiment. Langer et al. attributed the increase of non-radiative recombination to strain. An increase in the non-radiative A coefficient was also reported for laser structures by Strauß et al. [8] which they attributed to a reduced "QW quality" from blue to green.

The higher growth temperatures of blue QWs versus green would reduce point defect density (like carbon and vacancies). Indeed, two reports showed a strong increase of PL when increasing the QW growth temperature while keeping the same emission wavelength [10, 11]. The PL IQE curves in Hammersley et al. also show the maximum IQE is reached at lower powers for higher QW growth temperatures [10], which directly confirms smaller A coefficients at lower QW growth temperatures. A recent deep-level optical spectroscopy study found in green QWs about 10 times more deep levels roughly 1.5 eV below the gap than for blue QWs, and at the same time a later peak in PL-IQE, i.e. a higher A coefficient [38]. This deep level seems related to the lowest deep level which increased in HDD QWs [6], which corresponds with our observation of A for LDD green LEDs similar to A for all HDD LEDs. For single QWs on Si substrate (and thus with TDDs between LDD and HDD) a direct correlation between deep levels and high A coefficients has been demonstrated (unfortunately no emission wavelengths were given) [32]. Finally, a recent calculation of Shockley-Read-Hall recombination of $10^{16}\mathrm{cm}^{-2}$ gallium vacancy-oxygen complexes [35] agrees very well to our observed increase of the A coefficient towards 500 nm (black dashed line in fig. 5. However, at longer wavelength the energy difference to non-radiative states is no longer the non-radiative recombination rate limiting factor and saturates. This again indicates towards an increasing number of point defects beyond 500 nm.

Thus, the increase of A towards green for LDD LEDs is most likely caused by an enhanced non-radiative recombination at a deep level originating from point defects (e.g. carbon or vacancies) which are more incorporated at the lower growth temperatures needed for green QWs.

The B coefficients roughly follow the calculated squared wave function overlap of 3.0 nm InGaN QWs for all dislocation densities [line in fig. 5 (b)]. In case of B two main competing mechanism can either increase or reduce the radiative recombination, depending on the current density around the peak IQE used for the fitting.

The hole degeneracy decreases B for current densities exceeding typically $100\,\mathrm{A\,cm}^{-2}$ [23]. But those current densities are higher than the peak EQE (see fig. 2). On the other hand, the screening of the internal fields at higher carrier densities increases the wave function overlap [31, 36] and thus B. Assuming that all carriers in a QW contribute to screening, one can calculate the carrier density at peak IQE from eq. (8) and can then compare

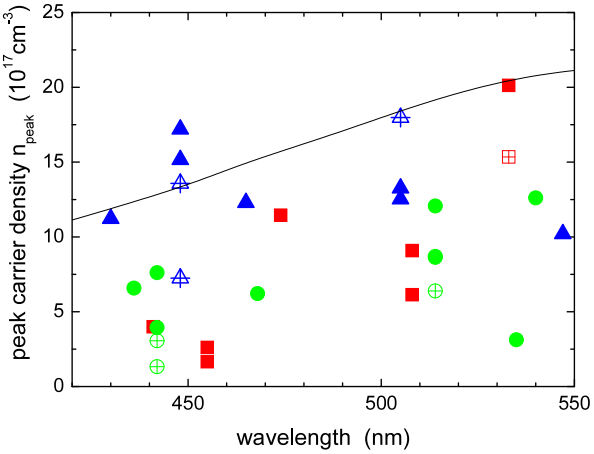

FIG. 6. Carrier densities $n_{peak} = \sqrt{A/C}$ at peak IQE for all LEDs and the calculated carrier density for a 10 % increase of the wave function overlap (line).

this to the calculated carrier density needed for a 10 % change of the overlap for 3 nm QWs. The results in fig. 6 show that all but one HDD LED device series at 448 nm are below a limit of 10 % increase of wave function overlap. Thus, the B coefficient obtained from fitting are hardly affected by screening below the peak IQE.

At very high currents the carrier density can reach much higher values. The typical operation point of 350 mA for a green LDD LED is equivalent to a carrier density of $n \approx 4 \times 10^{18}\mathrm{cm}^{-3}$ using the values from fig. 5. This would increase the calculated overlap by 23 % and via the square B by 50 % while blue-shifting the calculated emission by reasonable 8 nm. A comparable wavelength shift from peak EQE to maximum current was recently reported for long wavelength LEDs [39], supporting this estimation. Because B is low in the green region, carriers recombine slowly and accumulate more than in blue. The so increased carrier density and thus screening can explain the observed broadening of the EQE curves at the highest current densities observed in fig. 2 for the green LEDs.

Overall, we can confirm the results of Schiavon et al. that the B coefficients scales proportional to the squared wave function overlap [7]. Dislocations as well as point defects have no big effect on the B coefficient: the radiative recombination only depends on the QW thickness and In content.

C. Modelling

From fig. 5 we have obtained an ideal trend of the A, B, and C coefficients for low and high TDDs. With eq. (6) we can then calculate the IQE_{peak} for ideal devices.

For HDD, we kept A constant at $2 \times 10^7\,\mathrm{s}^{-1}$. For such a high A coefficient, the change of B due to the squared wave function overlap is enough to explain the reduction of the peak IQE from 90% at 400 nm to 23% at 540 nm

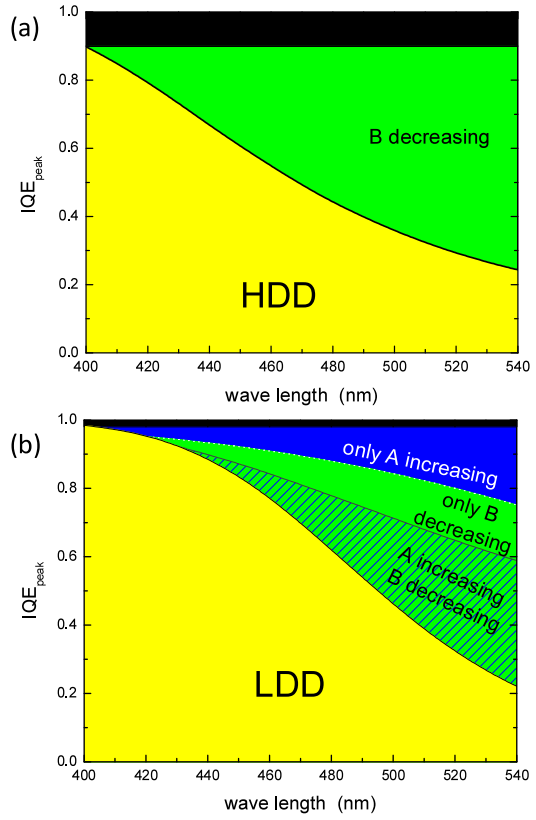

FIG. 7. Calculated peak IQE (solid) from eq. (6) using the coefficients from fig. 5 for (a) HDD LEDs with a fixed $A = 2 \times 10^7 \mathrm{s}^{-1}$ and (b) LDDs LEDs.

in fig. 7 (a). Thus, for high dislocation densities the green gap is indeed caused by the reduced wave function overlap.

However, when the A coefficient is much lower at the best LDD values of $10^6\,\mathrm{s}^{-1}$ ["only B decreasing" in fig. 7 (b)] then the peak IQE reduces much less, from 95% to 58%. If B is left unchanged at $10^{-10}\,\mathrm{cm}^3\mathrm{s}^{-1}$ (the 420 nm value) and only A increases according to fig. 5 (a), then the peak IQE reduces from 95% to 75% ["only A increasing" in fig. 7 (b)]. Only if both A increases and B decreases, then the peak IQE reduces from 95% at 400 nm to 22% at 540 nm, the typical values reported in literature (cf. EQE at 20 mA in [40, 41]).

Hence the reduction of the IQE towards green on low dislocation templates is not only caused by the reduction of the wave function overlap (i.e. radiative recombination B), but also to due to a strong increase of A. In other words, non-radiative recombination at defects, most likely point defects, is a strong contribution to the reduction of the IQE towards green, whereas dislocations even in the $10^9\,\mathrm{cm}^{-3}$ range do not limit the IQE in the green. This is supported by a recent publication which showed that the growth temperature of a QW strongly affects the IQE as measured by photoluminescence [10]. Furthermore, the deep levels signals in spectroscopy typical for HDD are also reached on LDD by QW grown at lower temperature to incorporate more In [6, 38]. If we could produce green QWs with a similar non-radiative recombination rate as for blue QWs, then a peak IQE close to 60 % would be possible even for green QWs [shaded area in fig. 7 (b)].

IV. CONCLUSION

From measuring the EQE curves of LEDs with different defect densities which emit from 450 nm to 540 nm, we conclude that dislocations mainly increase the non-radiative recombination in the blue wavelength region. The radiative recombination follows the calculated squared wave function overlap. Using the experimental ABC coefficients to model LEDs with different dislocations densities strongly suggests that non-radiative recombination is an important factor to the green gap. Hence, the performance of green LEDs cannot be improved to match that of blue LEDs only by reducing the polarisation fields. Point defects and other sources of non-radiative recombination must also be addressed.

ACKNOWLEDGMENTS

This work was supported by UK Engineering and Physics Scientific Research Council grants No EP/K008323/1 and EP/I012591/1.

[1] M. F. Schubert, S. Chhajed, J. K. Kim, E. F. Schubert, D. D. Koleske, M. H. Crawford, S. R. Lee, A. J. Fischer, G. Thaler, and M. A. Banas, Appl. Phys. Lett. **91**, 231114 (2007).
[2] X. A. Cao, Y. Yang, and H. Guo, J. Appl. Phys. **104**, 093108 (2008).
[3] K.-W. Liu, S.-J. Chang, S.-J. Young, T.-H. Hsueh, H. Hung, Y.-C. Mai, S.-M. Wang, and Y.-Z. Chen, J. Electrochem. Soc. **158**, H983 (2011).
[4] S. Kimura, J. Tajima, H. Nago, T. Hikosaka, H. Yoshida, K. Uesugi, and S. Nunoue, Proc. SPIE **8986**, 89861H (2014).
[5] Y. Harada, T. Hikosaka, S. Kimura, M. Sugai, H. Nago, K. Tachibana, N. Sugiyama, and S. Nunoue, Proc. SPIE **8278**, 82780J (2012).
[6] A. Armstrong, T. A. Henry, D. D. Koleske, M. H. Crawford, K. R. Westlake, and S. R. Lee, Appl. Phys. Lett. **101**, 162102 (2012).
[7] D. Schiavon, M. Binder, M. Peter, B. Galler, P. Drechsel, and F. Scholz, phys. stat. sol. (b) **250**, 283 (2013).
[8] U. Strauß, T. Hager, G. Brüderl, T. Wurm, A. Somers, C. Eichler, C. Vierheilig, A. Löffler, J. Ristic, and

A. Avramescu, Proc. SPIE **8986**, 89861L (2014).
[9] T. Langer, H. Jönen, A. Kruse, H. Bremers, U. Rossow, and A. Hangleiter, Appl. Phys. Lett. **103**, 022108 (2013).
[10] S. Hammersley, M. J. Kappers, F. C.-P. Massabuau, S.-L. Sahonta, P. Dawson, R. A. Oliver, and C. J. Humphreys, Appl. Phys. Lett. **107**, 132106 (2015).
[11] C.-F. Huang, T.-C. Liu, Y.-C. Lu, W.-Y. Shiao, Y.-S. Chen, J.-K. Wang, C.-F. Lu, and C. C. Yang, J. Appl. Phys. **104**, 123106 (2008).
[12] S. D. Bakshi, J. Sumner, M. Kappers, and R. Oliver, J. Crystal Growth **311**, 232 (2009).
[13] R. Oliver, M. Kappers, J. Sumner, R. Datta, and C. Humphreys, J. Crystal Growth **289**, 506 (2006).
[14] R. A. Oliver, F. C.-P. Massabuau, M. J. Kappers, W. A. Phillips, E. J. Thrush, C. C. Tartan, W. E. Blenkhorn, T. J. Badcock, P. Dawson, M. A. Hopkins, D. W. E. Allsopp, and C. J. Humphreys, Appl. Phys. Lett. **103**, 141114 (2013).
[15] F. C.-P. Massabuau, M. J. Davies, F. Oehler, S. K. Pamenter, E. J. Thrush, M. J. Kappers, A. Kovács, T. Williams, M. A. Hopkins, C. J. Humphreys, P. Dawson, R. E. Dunin-Borkowski, J. Etheridge, D. W. E. Allsopp, and R. A. Oliver, Appl. Phys. Lett. **105**, 112110 (2014).
[16] M. Pristovsek, Appl. Phys. Lett. **102**, 242105 (2013).
[17] H.-Y. Ryu, H.-S. Kim, and J.-I. Shim, Appl. Phys. Lett. **95**, 081114 (2009).
[18] Q. Dai, Q. Shan, J. Wang, S. Chhajed, J. Cho, E. F. Schubert, M. H. Crawford, D. D. Koleske, M.-H. Kim, and Y. Park, Appl. Phys. Lett. **97**, 133507 (2010).
[19] B. Galler, H.-J. Lugauer, M. Binder, R. Hollweck, Y. Folwill, A. Nirschl, A. Gomez-Iglesias, B. Hahn, J. Wagner, and M. Sabathil, Appl. Phys. Express **6**, 112101 (2013).
[20] Y. C. Shen, G. O. Mueller, S. Watanabe, N. F. Gardner, A. Munkholm, and M. R. Krames, Appl. Phys. Lett. **91**, 141101 (2007).
[21] S. Schulz, M. A. Caro, C. Coughlan, and E. P. O'Reilly, Phys. Rev. B **91**, 035439 (2015).
[22] A. Morel, P. Lefebvre, S. Kalliakos, T. Taliercio, T. Bretagnon, and B. Gil, Phys. Rev. B **68**, 045331 (2003).
[23] S. Karpov, Opt. Quant. Electron. **47**, 1293 (2015).
[24] T. J. Badcock, M. Ali, T. Zhu, M. Pristovsek, R. A. Oliver, and A. J. Shields, Appl. Phys. Lett. **109**, 151110 (2016).
[25] A. David, C. A. Hurni, N. G. Young, and M. D. Craven, Appl. Phys. Lett. **109**, 033504 (2016); **109**, 099902 (2016).
[26] F. Nippert, S. Karpov, I. Pietzonka, B. Galler, A. Wilm, T. Kure, C. Nenstiel, G. Callsen, M. Straßburg, H.-J. Lugauer, and A. Hoffmann, Jpn. J. Appl. Phys. **55**, 05FJ01 (2016).
[27] J. Hader, J. V. Moloney, and S. W. Koch, Appl. Phys. Lett. **96**, 221106 (2010).
[28] H. Zhao, G. Liu, R. A. Arif, and N. Tansu, Solid-State Electronics **54**, 1119 (2010).
[29] A. David, C. A. Hurni, N. G. Young, and M. D. Craven, Appl. Phys. Lett. **109**, 083501 (2016).
[30] C. van Opdorp and G. W. 't Hooft, J. Appl. Phys. **52**, 3827 (1981).
[31] P. G. Eliseev, M. Osin'ski, H. Li, and I. V. Akimova, Appl. Phys. Lett. **75**, 3838 (1999).
[32] C. D. Santi, M. Meneghini, M. L. Grassa, B. Galler, R. Zeisel, M. Goano, S. Dominici, M. Mandurrino, F. Bertazzi, D. Robidas, G. Meneghesso, and E. Zanoni, J. Appl. Phys. **119**, 094501 (2016).
[33] M. Meneghini, N. Trivellin, G. Meneghesso, E. Zanoni, U. Zehnder, and B. Hahn, J. Appl. Phys. **106**, 114508 (2009).
[34] J. Wang, T. Meisch, D. Heinz, R. Zeller, and F. Scholz, phys. stat. sol. (b) **253**, 174 (2016).
[35] A. Alkauskas, C. E. Dreyer, J. L. Lyons, and C. G. Van de Walle, Phys. Rev. B **93**, 201304 (2016).
[36] R. P. Green, J. J. D. McKendry, D. Massoubre, E. Gu, M. D. Dawson, and A. E. Kelly, Appl. Phys. Lett. **102**, 091103 (2013).
[37] A. David and M. J. Grundmann, Appl. Phys. Lett. **96**, 103504 (2010).
[38] A. M. Armstrong, M. H. Crawford, and D. D. Koleske, Appl. Phys. Express **7**, 032101 (2014).
[39] S. Saito, R. Hashimoto, J. Hwang, and S. Nunoue, Appl. Phys. Express **6**, 111004 (2013).
[40] L. Jun-Lin, Z. Jian-Li, W. Guang-Xu, M. Chun-Lan, X. Long-Quan, D. Jie, Q. Zhi-Jue, W. Xiao-Lan, P. Shuan, Z. Chang-Da, W. Xiao-Ming, F. Wen-Qing, and J. Feng-Yi, Chin. Phys. B **24**, 067804 (2015).
[41] M. Pristovsek, C. J. Humphreys, S. Bauer, M. Knab, K. Thonke, G. Kozlowski, D. O'Mahony, P. Maaskant, and B. Corbett, Jpn. J. Appl. Phys. **55**, 05FJ10 (2016).